J|A|C|S
ARTICLES
Published on Web 02/04/2005

Structure−Property Relationships of Donor/Acceptor-Functionalized Tetrakis(phenylethynyl)benzenes and Bis(dehydrobenzoannuleno)benzenes

Jeremiah A. Marsden, Jeremie J. Miller, Laura D. Shirtcliff, and Michael M. Haley*

Contribution from the Department of Chemistry and Materials Science Institute, University of Oregon, Eugene, Oregon 97403-1253

Received September 24, 2004; E-mail: haley@uoregon.edu

Abstract: A series of tetrakis(phenylethynyl)benzenes and bis(dehydrobenzoannuleno)benzenes have been synthesized containing tetra-substitutions of neutral, donor, and mixed donor/acceptor groups. To ascertain the importance of substitutional and structural differences of the phenylacetylenes, the optical absorption and emission properties of each series were examined. Conjugation effectiveness, electron density, planarity, and geometry of charge-transfer pathways were found to have a pronounced effect on the overall optical and material properties. Considerable self-association behavior due to face-to-face stacking in solution was observed for donor/acceptor-functionalized macrocycles and was quantified by concentration-dependent ^{1}H NMR measurements. A solvent-dependent polymerization of one macrocycle regioisomer was observed and characterized. To provide further insight into the energy levels and electronic transitions present, computational studies of each system were performed.

Introduction

Organic compounds possessing a high degree of conjugation have long been recognized as ideal materials for advanced electronic and photonic applications including organic LEDs, liquid crystal displays, thin film transistors, solar cells, and optical storage devices.[1−3] Changes in the substitutional groups and substitution pattern, conjugation, and molecular electronic structure can bring about very different optical and physical properties for such materials.[2−7] To design an organic molecule with a specific application in mind, knowledge of the material's structure−property relationship is necessary. With this understanding, the ability to "tune" a class of materials to enhance an explicit property can be achieved.

Functionalized cruciform-conjugated phenylacetylene and phenylvinylene structures are known to exhibit remarkable optical and electronic properties because of their multiple conjugated pathways.[2,6−9] Possessing this cruciform-type structure, 1,2,4,5-tetrakis(phenylethynyl)benzenes (TPEBs) provide an ideal carbon framework for studying the intrinsic effect of functional group substitution on each conjugated pathway and on the overall material properties of each system. Substitution of electron donor and/or acceptor groups at the 4′-positions gives rise to discreet two-dimensional π-chromophores. By varying the substitution pattern of the donor and acceptor groups, each individual charge-transfer pathway can be enhanced. We[10−12]

(1) (a) Chen, J.; Reed, M. A.; Dirk, S. M.; Price, D. W.; Rawlett, A. M.; Tour, J. M.; Grubisha, D. S.; Bennett, D. W. *NATO Sci. Ser. II: Math., Phys., Chem.* **2003**, *96*, 59−195. (b) Domerco, B.; Hreha, R. D.; Zhang, Y.-D.; Haldi, A.; Barlow, S.; Marder, S. R.; Kippelen, B. *J. Polym. Sci., Part B: Polym. Phys.* **2003**, *41*, 2726−2732. (c) Shirota, Y. *J. Mater. Chem.* **2000**, *10*, 1−25. (d) *Photonic and Optoelectronic Polymers*; Jenekhe, S. A., Wynne, K. J., Eds.; American Chemical Society: Washington, DC, 1995. (e) Special Issue: *Chem. Rev.* **1994**, *94*, 1−278. (f) *Conjugated Polymers and Related Materials. The Interconnection of Chemical and Electronic Structure*; Lunström, W. R., Salaneck, I., Rånby, B., Eds.; Oxford University Press: Oxford, 1993.

(2) Nielsen, M. B.; Diederich, F. In *Modern Arene Chemistry*; Astruc, D., Ed.; Wiley-VCH: Weinheim, Germany, 2002; pp 196−216.

(3) Cornil, J.; Beljonne, D.; Calbert, J.-P.; Brédas, J.-L. *Adv. Mater.* **2001**, *13*, 1053−1067.

(4) Inter alia: (a) Boydston, A. J.; Yin, Y.; Pagenkopf, B. L. *J. Am. Chem. Soc.* **2004**, *126*, 3724−3725. (b) Wong, M. S.; Li, Z. H.; Tao, Y.; D'Iorio, M. *Chem. Mater.* **2003**, *15*, 1198−1203. (c) van Mullekom, H. A. M.; Vekemans, J. A. J. M.; Havinga, E. E.; Meijer, E. W. *Mater. Sci. Eng., R* **2001**, *R32*, 1−40. (d) Tykwinski, R. R.; Hilger, A.; Diederich, F.; Luthi, H. P.; Seiler, P.; Gramlich, V.; Gisselbrecht, J.-P.; Boudon, C.; Gross, M. *Helv. Chim. Acta* **2000**, *83*, 1484−1508. (e) Cammi, R.; Mennucci, B.; Tomasi, J. *J. Am. Chem. Soc.* **1998**, *120*, 8834−8847. (f) Moore, A. J.; Bryce, M. R.; Batsanov, A. S.; Green, A.; Howard, J. A. K.; McKervey, A.; McGuigan, P.; Ledoux, I.; Orti, E.; Viruela, R.; Viruela, P. M.; Tarbit, B. *J. Mater. Chem.* **1998**, *8*, 1173−1184. (g) Bourhill, G.; Brédas, J.-L.; Cheng, L.-T.; Marder, S. R.; Meyers, F. M.; Perry, J. W.; Tiemann, B. G. *J. Am. Chem. Soc.* **1994**, *116*, 2619−2620.

(5) Jayakannan, M.; Van Hal, P. A.; Janssen, R. A. J. *J. Polym. Sci., Part A: Polym. Chem.* **2001**, *40*, 251−261.

(6) Tykwinski, R. R.; Schreiber, M.; Carlón, R. P.; Diederich, F.; Gramlich, V. *Helv. Chim. Acta* **1996**, *79*, 2249−2280.

(7) Tykwinski, R. R.; Schreiber, M.; Gramlich, V.; Seiler, P.; Diederich, F. *Adv. Mater.* **1996**, *8*, 226−31.

(8) (a) Wilson, J. N.; Hardcastle, K. I.; Josowicz, M.; Bunz, U. H. F. *Tetrahedron* **2004**, *60*, 7157−7167. (b) Wilson, J. N.; Smith, M. D.; Enkelmann, V.; Bunz, U. H. F. *Chem. Commun.* **2004**, 1700−1701. (c) Wilson, J. N.; Josowicz, M.; Wang, Y.; Bunz, U. H. F. *Chem. Commun.* **2003**, 2962−2963. (d) Miteva, T.; Palmer, L.; Kloppenburg, L.; Neher, D.; Bunz, U. H. F. *Macromolecules* **2000**, *33*, 652−654.

(9) (a) Ojima, J.; Kakumi, H.; Kitatani, K.; Wada, K.; Ejiri, E.; Nakada, T. *Can. J. Chem.* **1984**, *63*, 2885−2891. (b) Ojima, J.; Enkaku, M.; Uwai, C. *Bull. Chem. Soc. Jpn.* **1977**, *50*, 933−935.

(10) (a) Marsden, J. A.; Palmer, G. J.; Haley, M. M. *Eur. J. Org. Chem.* **2003**, 2355−2369. (b) Jones, C. S.; O'Connor, M. J.; Haley, M. M. In *Acetylene Chemistry: Chemistry, Biology, and Materials Science*; Diederich, F., Tykwinski, R. R., Stang, P. J., Eds.; Wiley-VCH: Weinheim, Germany, 2004; pp 303−385.

(11) (a) Wan, W. B.; Haley, M. M. *J. Org. Chem.* **2001**, *66*, 3893−3901. (b) Wan, W. B.; Brand, S. C.; Pak, J. J.; Haley, M. M. *Chem.−Eur. J.* **2000**, *6*, 2044−2052.

(12) Pak, J. J.; Weakley, T. J. R.; Haley, M. M. *J. Am. Chem. Soc.* **1999**, *121*, 8182−8192.

10.1021/ja044175a CCC: $30.25

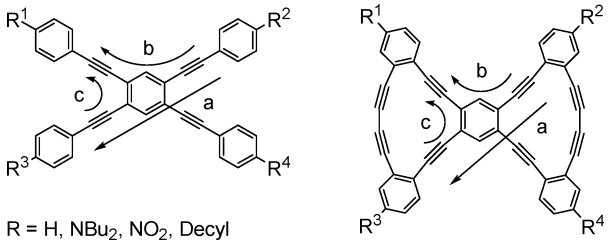

Figure 1. Conjugated pathways present in the TPEB and DBA systems.

and others[5−9,13,14] have previously identified linear conjugation between donor and acceptor groups as ideal for lowering the HOMO−LUMO gap for charge-transfer, thereby enhancing the optical and nonlinear optical (NLO) properties of the material. The TPEB framework provided us with an ideal system for studying the differences between the linear-conjugated (Figure 1, path a), cross-conjugated (path b), and "bent" conjugated (path c) pathways to gain a better understanding of the geometrical aspects of the charge-transfer pathways in phenylacetylene networks.

We have also long been interested in the effect of planarity on the conjugation of donor/acceptor-functionalized systems. Because of the nearly free rotation about the phenyl−ethynyl bonds in the TPEB systems, conjugation may be disrupted. Therefore, we have designed a series of bis(dehydrobenzoannuleno)benzenes (bisDBAs), which possess the same basic carbon backbone as the TPEBs, yet are locked into planarity by a diacetylene bridge, providing an ideal system for direct comparison of conjugation effectiveness (Figure 1).[8d,9,10] We have previously studied the consequences of donor and acceptor substitution patterns in dodecadehydro[18]annulenes on the optical and NLO properties of DBAs.[12,15] Because of the symmetry constraints of these monoannulene systems, however, placement of functional groups was somewhat limited, and isolation of the exact effects due to each unique chromophore proved difficult. The new bisannulene and TPEB systems described in this article, on the other hand, provide a more rational approach to functional group placement at each of four equivalent positions on the periphery of the conjugated cruciform backbone. With functionalization at each of these positions, the entire phenylacetylene framework contributes to the overall conjugation in each system (with only minimal contribution from the diacetylene bridge of the DBAs), allowing discrete identification of property changes due only to differences in substitution pattern. By studying analogous substitution patterns between the TPEB and DBA systems, we hope to determine the consequence of planarity on conjugation effectiveness. Since the DBA systems should demonstrate better overall conjugation, their optical and nonlinear optical properties should also be enhanced.

In this article, we describe the synthesis and full characterization of a series of donor- and acceptor-functionalized nonplanar tetrakis(phenylethynyl)benzenes and their planar bis(dehydrobenzo[14]- and [15]annuleno)benzene counterparts. For control comparisons, the tetra-donor and neutral tetra-decyl-substituted compounds have also been prepared and analyzed. The optical absorption and emission characteristics of these systems were examined for structure−function relationships. We herein also report a computational study of the conjugation effectiveness of each system through geometry optimization and molecular orbital plots analysis. Last, the aggregation properties of the donor/acceptor-functionalized bisDBAs are described.

Results and Discussion

Synthesis. The general synthetic strategy for the phenylacetylene series relied heavily on the Sonogashira cross-coupling protocol, for which the reactivity difference between aryl iodides and aryl bromides allowed specific placement of the donor and acceptor units.[16] At the heart of each molecule was a central tetrahaloarene to which both triisopropylsilyl (TIPS)- and trimethylsilyl (TMS)-protected alkynes were attached for the TPEB syntheses. Likewise, donor- and/or acceptor-functionalized diethynylarenes were selectively cross-coupled to the central tetrahaloarenes for the DBA syntheses. For the ring closure of the annulene systems, we employed both Cu-mediated[17] as well as oxidative Pd-catalyzed[18] homocoupling to control selectivity of the ring geometry.[19]

The target TPEBs are shown in Figure 2, which consist of the known parent compound (**1**),[14] tetra-donor (**2**), and each of three regioisomers containing two donor and two acceptor groups with like substituents fused either ortho (**3**), meta (**4**), or para (**5**) to each other.[20] The assembly of TPEB **2** is shown in Scheme 1. Phenylacetylene **6** was made by Sonogashira cross-coupling of trimethylsilylacetylene (TMSA) with *N*,*N*-dibutyl-4-iodoaniline.[12] The silyl protecting group was next removed with TBAF, and after a 4-fold cross-coupling with 1,2,4,5-tetraiodobenzene, tetra-donor **2** was isolated.

The syntheses of the donor- and acceptor-functionalized TPEBs are exemplified in Scheme 2 with the synthesis of phenylacetylene **3**. Direct cross-coupling of the phenylacetylenes as in Scheme 1 was initially attempted, but proved inconsistent and low yielding. Improved results were attained through sequential installation of silyl-protected acetylenes to the central ring followed by attachment of the donor- and acceptor-substituted arenes. Starting from 1,2-dibromo-4,5-diiodobenzene **7**,[21] TMSA was first cross-coupled to the more reactive iodo positions to give **8**, followed by a second cross-coupling of TIPSA to the remaining bromo positions at an elevated temperature, providing **9** in 75% for the two steps. The selectivity of the silane protective groups came into play next, as the TMS group was preferentially removed with K_2CO_3/MeOH and the resulting alkyne was cross-coupled with *N*,*N*-dibutyl-4-iodoaniline to give **10**. Finally, deprotection of the

(13) Hilger, A.; Gisselbrecht, J. P.; Tykwinski, R. R.; Boudon, C.; Schreiber, M.; Martin, R. E.; Lüthi, H. P.; Gross, M.; Diederich, F. *J. Am. Chem. Soc.* **1997**, *119*, 2069−2078.
(14) Kondo, K.; Yasuda, S.; Tohoru, S.; Miya, M. *J. Chem. Soc., Chem. Commun.* **1995**, 55−56.
(15) Sarkar, A.; Pak, J. J.; Rayfield, G. W.; Haley, M. M. *J. Mater. Chem.* **2001**, *11*, 2943−2945.
(16) (a) Marsden, J. A.; Haley, M. M. In *Metal-Catalyzed Cross-Coupling Reactions*, 2nd ed.; de Meijere, A., Diederich, F., Eds.; Wiley-VCH: Weinheim, Germany, 2004; pp 317−394. (b) Sonogashira, K. In *Metal-Catalyzed Cross-Coupling Reactions*; Diederich, F., Stang, P. J., Eds.; Wiley-VCH: Weinheim, Germany, 1998; pp 203−230.
(17) Siemsen, P.; Livingston, R. C.; Diederich, F. *Angew. Chem., Int. Ed.* **2000**, *39*, 2632−2657.
(18) (a) Marsden, J. A.; O'Connor, M. J.; Haley, M. M. *Org. Lett.* **2004**, *6*, 2385−2388. (b) Lei, A.; Srivastava, M.; Zhang, X. *J. Org. Chem.* **2002**, *67*, 1969−1971. (c) Liu, Q.; Burton, D. J. *Tetrahedron Lett.* **1997**, *38*, 4371−4374. (d) Takano, S.; Sugihara, T.; Ogasawara, K. *Synlett* **1990**, 453−454. (e) Rossi, R.; Carpita, A.; Bigelli, C. *Tetrahedron Lett.* **1985**, *26*, 523−526.
(19) Marsden, J. A.; Miller, J. J.; Haley, M. M. *Angew. Chem., Int. Ed.* **2004**, *43*, 1694−1697.
(20) Miller, J. J.; Marsden, J. A.; Haley, M. M. *Synlett* **2004**, 165−168.
(21) Miljanic, O. S.; Vollhardt, K. P. C.; Whitener, G. D. *Synlett* **2003**, 29−30.

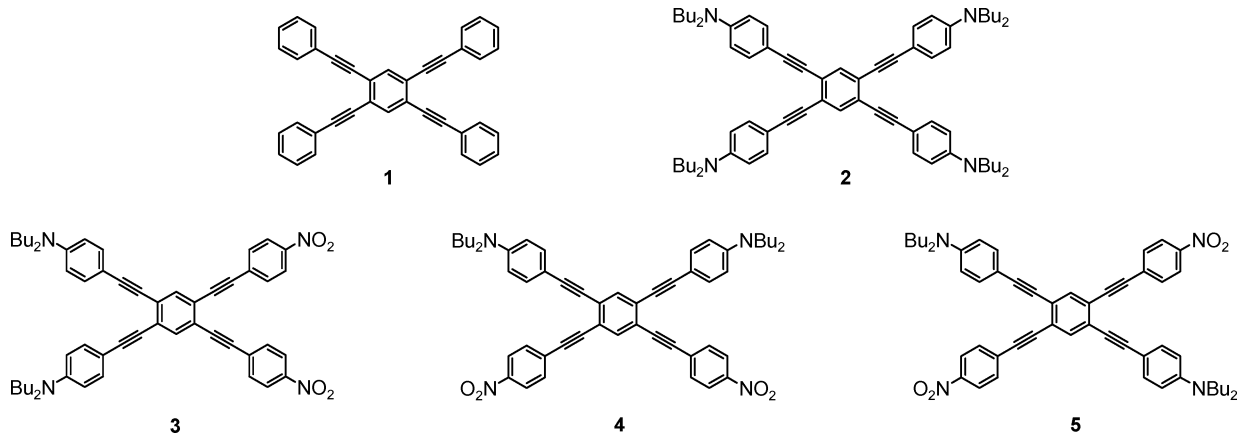

Figure 2. Target TPEBs **1**−**5**.

Scheme 1. Preparation of TPEB **2**[a]

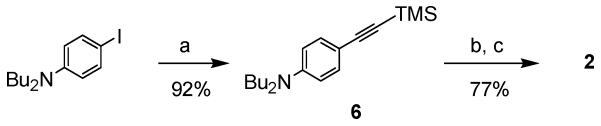

[a] Conditions: (a) TMSA, $Pd(PPh_3)_2Cl_2$, CuI, DIPA, THF; (b) K_2CO_3, THF, MeOH; (c) 1,2,4,5-tetraiodobenzene, $Pd(PPh_3)_4$, CuI, DIPA, THF, 40 °C.

Scheme 2. Synthesis of TPEB **3**[a]

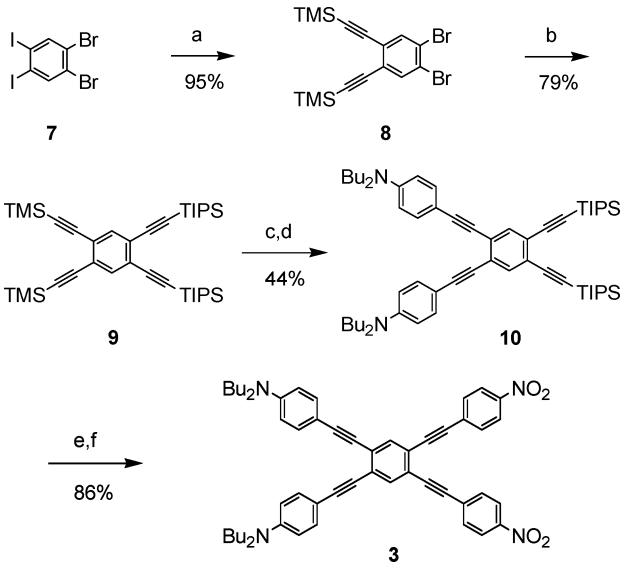

[a] Conditions: (a) TMSA, $Pd(PPh_3)_2Cl_2$, CuI, DIPA, THF; (b) TIPSA, $Pd(PPh_3)_2Cl_2$, CuI, DIPA, THF, 60 °C; (c) K_2CO_3, THF, MeOH; (d) *N*,*N*-dibutyl-4-iodoaniline, $Pd(PPh_3)_4$, CuI, DIPA, THF; (e) TBAF, THF; (f) 4-iodo-1-nitrobenzene, $Pd(PPh_3)_4$, CuI, DIPA, THF.

TIPS groups with TBAF and coupling of the resultant terminal alkyne with 4-iodo-1-nitrobenzene afforded TPEB **3** as a red powder. The remaining isomers **4** and **5** followed analogous synthetic schemes with yields as reported in Table 1.[22]

The synthetic strategy for construction of the DBA systems is outlined in Scheme 3. As we have previously reported for similar annulenic systems,[19] we can control ring size and geometry of the DBAs through the cyclization technique, thereby making either bis[15]annulenes (**A**) with cyclization across the meta-fused alkynes or bis[14]annulenes (**B**) cyclized across the ortho-fused alkynes from the same precursor (**C**).

(22) See Supporting Information for details.

Table 1. Yields for Syntheses of TPEBs **3**−**5**

Haloarene	Step a	Step b	Steps c,d	Steps e,f	TBED
	95%	79%	44%	86%	**3**
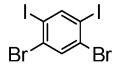	82%	99%	35%	67%	**4**
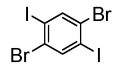	90%	74%	42%	78%	**5**

This selectivity between bisDBAs is controlled through the conditions used for cyclization: Cu-mediated vs Pd-catalyzed homocoupling of the alkynes, vide infra. Precursor **C** is made by a convergent synthesis consisting of sequential cross-couplings of the decyl, donor, and/or acceptor diynes (**D**) to the central tetrahaloarene (**E**). The target series of bis(dehydrobenzo[14]- and [15]annulene)benzenes is shown in Figure 3. Analogous to the TPEB systems, the DBAs consist of neutral pure hydrocarbons **11** and **12** substituted with decyl groups to improve solubility, tetra-donors **13** and **14**, and the series of donor- and acceptor-functionalized bis[14]- and [15]annulenes **15**−**20**.

The diyne units (**21a**−**c**) were made from known iodoarenes **22a**−**c**[11,12] through a simple cross-coupling with TMSA followed by deprotection of the TMS group (Scheme 4). The precursors to cyclization (**23a**,**b**) for the tetra-decyl and tetra-donor systems were assembled by 4-fold Sonogashira coupling of diynes **21a** or **21b** with 1,2,4,5-tetraiodobenzene. Because of anticipated solubility issues, the tetra-acceptor systems were not attempted.

The syntheses of the donor/acceptor-substituted cyclization precursors start with three regioisomers of dibromodiiodobenzene as exemplified by the assembly of **24** (Scheme 5). Cross-coupling of 2 equiv of nitro-diyne **21c** to the iodo positions of **7** gave the electron-deficient dibromoarene **25**. Since alkyne cross-couplings are known to favor electron-poor haloarenes and electron-rich alkynes,[16] this set up an ideal system for the second coupling of donor diyne **21b** to the bromo positions. As a result, a moderate temperature of only 60 °C was required to provide precursor **24** in a very good 76% yield. Using this synthetic methodology, we also constructed the precursors to annulenes **16**, **17**, **19**, and **20** with the yields reported in Table 2.[22]

Scheme 3

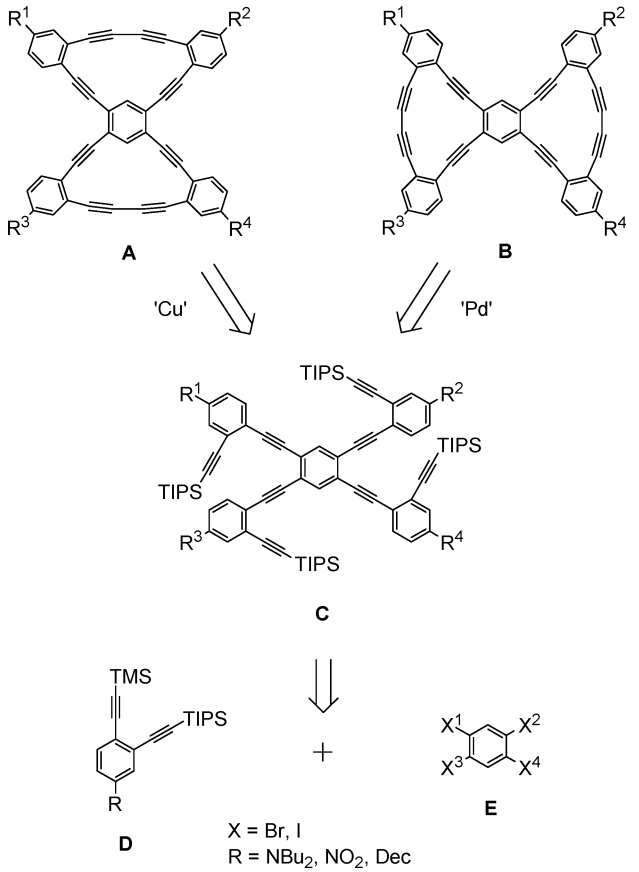

As we have recently reported and noted above, upon cyclization an interesting selectivity for ring formation based upon the cyclization conditions employed was discovered.[19] This selectivity is illustrated for the cyclization of the tetra-donor precursor **23b** (Scheme 6). After deprotection of the silanes, intramolecular homocoupling under Glaser or Eglinton conditions with Cu−pyridine gave exclusively the bis[15]annulene **13** (70%), which is cyclized across the meta fusion of alkyne units. An often overlooked consideration when performing this type of reaction is the geometry of the Cu−acetylide prior to reductive elimination. The most commonly accepted mechanistic picture for this sequence involves a pseudo-trans configuration involving a dimeric Cu(I)−acetylide (**A**, Scheme 7).[23] Not surprisingly, on the basis of simple molecular modeling calculations,[24] formation of the bis[15]annulene adopts a trans-like configuration of the alkynes for ideal ring closure. Conversely, for cyclization across the ortho-fused alkynes, as in bis[14]-annulene (**14**), a cis-like geometry is favored. To enforce this cis geometry in the system, we turned to oxidative palladium chemistry.[18] A key benefit of a Pd-homocoupling procedure is the ability to fine-tune the catalytic system by the judicious choice of ligand. A cis addition of the acetylides to the Pd center could be enforced with cis-bidentate ligated Pd(dppe)Cl_2 (dppe = diphenylphosphinoethane) (**B**, Scheme 7), resulting in exclusively bis[14]annulene **14** in a respectable 84% yield (Scheme 6). On the other hand, intramolecular homocoupling using monodentate PPh_3 ligands, which allows trans addition of the acetylides, showed preferential formation of the bis[15]-annulene, as expected, giving a 4:1 mixture of **13**:**14**.

We subjected all of the precursor polyynes to both the Cu−pyridine and Pd(dppe)Cl_2 methods in order to assemble the full series of bisannulenes shown in Figure 3. As outlined in Table 2, yields for the electron-rich tetra-donor systems were the highest, followed by moderate yields for the neutral DBAs, and poorer yields for the donor/acceptor systems. Even with very dilute conditions and slow injection of the deprotected polyyne, cyclization of the donor/acceptor-functionalized DBAs produced copious amounts of oligomeric byproduct because of competing intermolecular homocoupling. Therefore, despite numerous attempts at cyclization and modifications to the reaction conditions, construction of DBA **20** remained elusive, while all other DBA syntheses were successful.

As structural isomers, the bis[14]- and [15]annulenes have very similar spectral characteristics, making identification difficult. There was, however, one key difference in the ^{1}H NMR spectra between each pair of compounds. For example, the singlet from the two protons on the central ring of **13** and **14** displayed a marked difference in chemical shift, whether it was intraannular (bis[15]annulene **13**, $\delta = 8.42$ ppm) or between rings (bis[14]annulene **14**, $\delta = 8.24$ ppm).[25,26] On the basis of molecular modeling calculations,[24] the central protons of the bis[15]annulene are much closer to the internal alkyne units than the analogous protons on the bis[14]annulene because of the internal bowing of the phenyl−ethynyl bonds of **13**. Therefore, a larger anisotropic deshielding effect due to the proximitiy of the triple bonds gave the central protons of **13** a much more downfield shift than those of **14**. This trend continued for each substitution of annulene.[22] Proof that our structural assignments were correct was provided through definitive construction of **13** by cyclization of one ring at a time.[19] This route, which allowed no possibility for formation of 14-membered rings, afforded material possessing identical spectral characteristics.

Electronic Absorption Spectra. The UV−vis spectra of the TPEBs and DBAs provide a great deal of insight into the electronic structure of the systems. All of the TPEB systems display a characteristic pattern of two broad bands as seen in the pure hydrocarbon parent **1** (Figure 4, Table 3). With the added electron density of four NBu_2 groups, a large red-shift (∼60 nm) of both bands was observed for phenylacetylene **2** with a dramatic increase in the absorption of the lower energy peak. The corresponding bands of the donor/acceptor-substituted TPEB spectra are remarkably broadened and show further bathochromic shifts with absorption cutoffs extending beyond 550 nm, indicative of intramolecular charge-transfer transitions. An obvious difference is seen between each substitution pattern of the donor and acceptor groups. TPEBs **3** and **4**, which both possess linear-conjugated pathways, have a much more distinct low-energy band. Lacking this linear charge-transfer conduit, the analogous low-energy band of TPEB **5** is greatly weakened. This further indicates that linear-conjugated pathways are more efficient than the bent-conjugated or cross-conjugated donor to acceptor pathways present in **5**. A distinct correlation is also observed between the net dipole moments of the compounds

(23) Bohlmann, F.; Schönowsky, H.; Inhoffen, E.; Grau, G. *Chem. Ber.* **1963**, *97*, 794−800.
(24) PM3(tm) calculations performed on an SGI Octane workstation using Spartan SGI version 5.1.3 by Wavefunction, Inc.: Irvine, CA, 1998.
(25) Tobe, Y.; Kishi, J.; Ohki, I.; Sonoda, M. *J. Org. Chem.* **2003**, *68*, 3330−3332.
(26) Baldwin, K. P.; Matzger, A. J.; Scheiman, D. A.; Tessier, C. A.; Vollhardt, K. P. C.; Youngs, W. J. *Synlett* **1995**, 1215−1218.

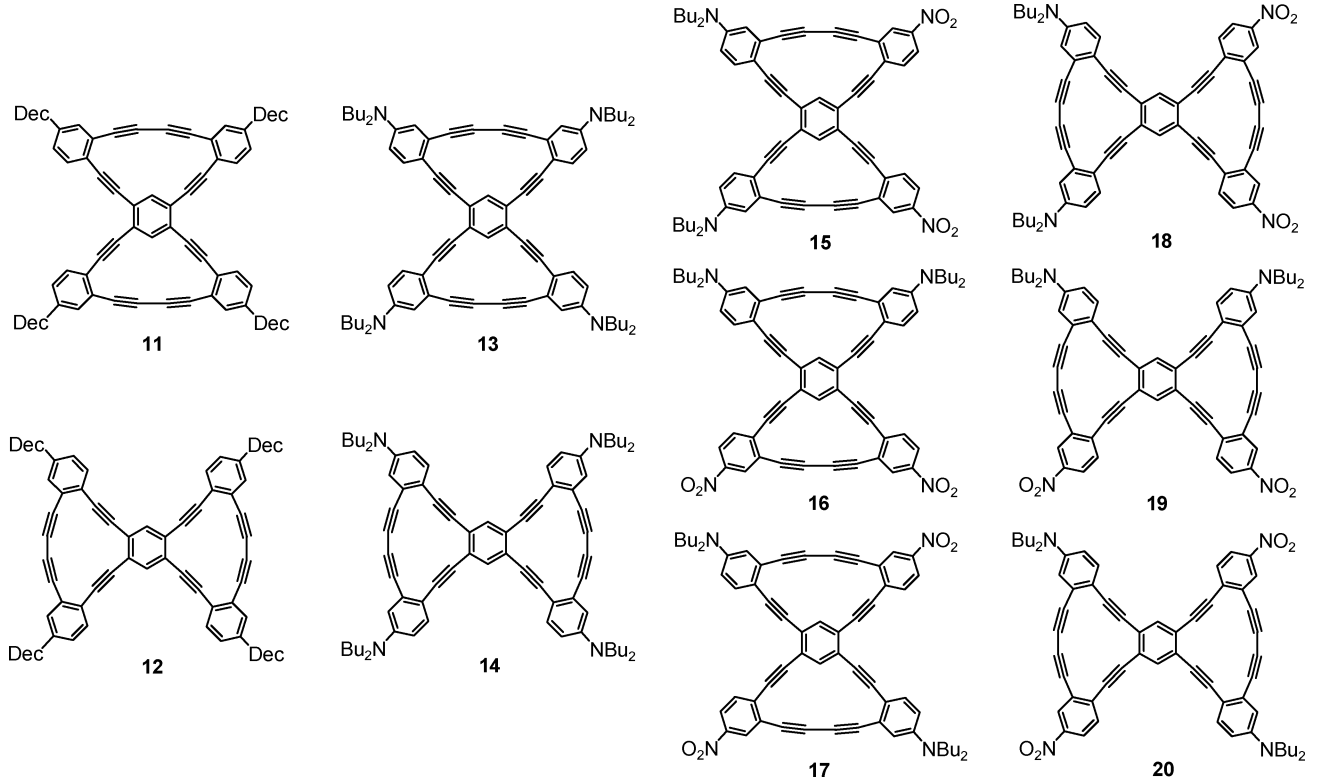

Figure 3. Target bisDBAs **11**−**20**.

Scheme 4

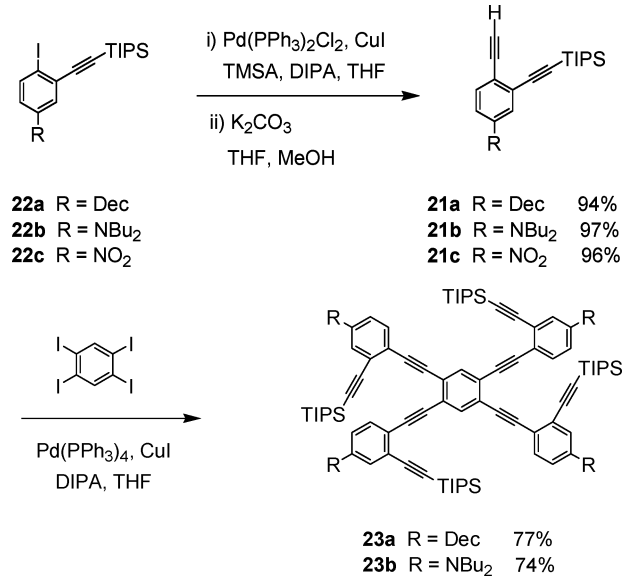

Scheme 5

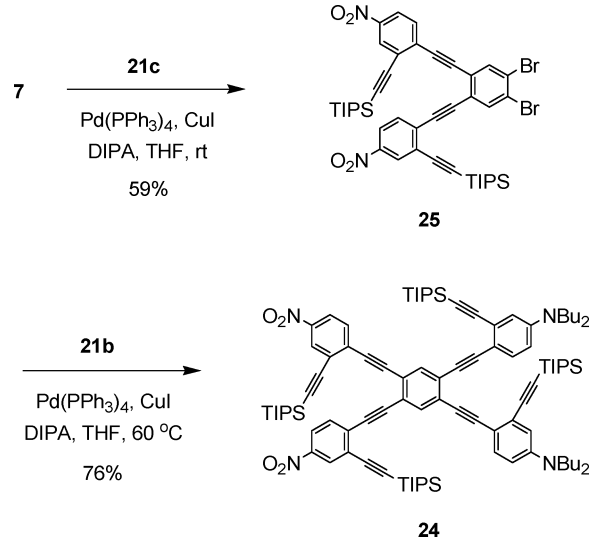

calculated using the B3LYP/6-31G* basis set and the extent of bathochromic shift (Table 3). The meta-substituted TPEB **4** possesses the largest dipole as well as the longest wavelength λ_{max}.

The effect of planarity on the cruciform framework was distinctly seen by UV−vis spectroscopy. The free rotation of the central phenyl−ethynyl bonds in **1** was eliminated in annulenes **11** and **12**, effectively locking the structures into planarity by the outer diacetylene bridge. Because of the resultant enhancement of conjugation in the DBAs, a perceptible bathochromic shift of the low-energy bands of ∼65 nm was observed (Figure 5, Table 3). Interestingly, there was a great difference in the fine structure of the absorption bands between bis[14]- and [15]annulene topologies. The larger extinction coefficient and greater number of sharp peaks present in bis-[14]annulene **12** suggest that more complex vibronic transitions are at work. A reasonable explanation for this difference is due to the presence of a weak ring current in the aromatic 14-membered rings.[27] A similar degree of red-shift was detected for the tetra-donor annulenes **13** and **14** from TPEB **2**, although less fine structure is present in these systems than in the tetra-decyl-substituted DBAs (Figure 6). A noticeable difference between the bis[15]annulenes (**11** and **13**) and bis[14]annulenes

(27) (a) Boydston, A. J.; Haley, M. M.; Williams, R. V.; Armantrout, J. R. *J. Org. Chem.* **2002**, *67*, 8812−8819. (b) Bell, M. L.; Chiechi, R. C.; Johnson, C. A.; Kimball, D. B.; Matzger, A. J.; Wan, W. B.; Weakley, T. J. R.; Haley, M. M. *Tetrahedron* **2001**, *57*, 3507−3520.

Table 2. Yields for Syntheses of DBAs **11**−**20**

Haloarene	Acceptor Coupling	Donor Coupling	Cyclization	DBA
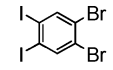	59%	76%	38%	**15**
			8%	**18**
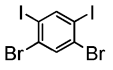	76%	86%	18%	**16**
			21%	**19**
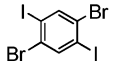	64%	87%	21%	**17**
			[a]	**20**
	77%[b]		58%	**11**
			55%	**12**
	[c]	74%	70%	**13**
			84%	**14**

[a] No detectable product formation. [b] Yield for tetra-decyl coupling. [c] Not applicable.

Scheme 6

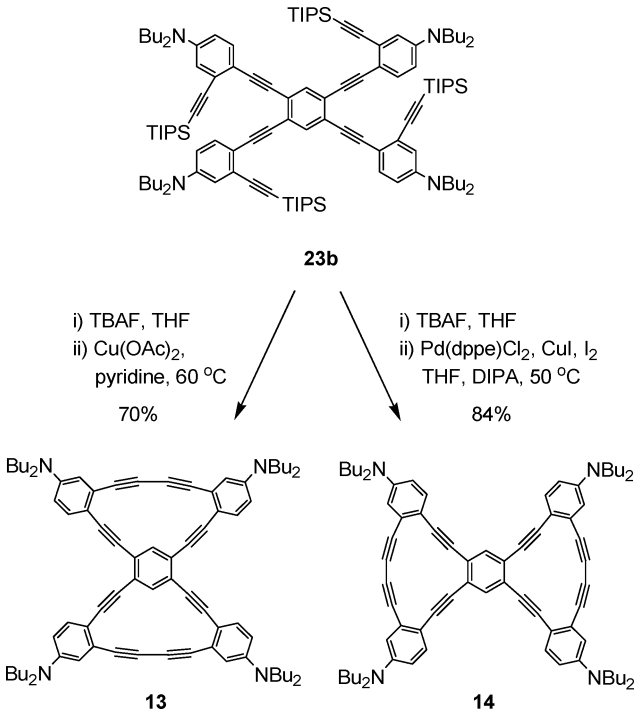

(**12** and **14**) was the higher absorption of the longest-wavelength λ_{max} in the bis[15]annulene systems. This rise in intensity may be due to the greater linearity of conjugated phenylacetylenic pathways present in **11** and **13**, while the alkynyl bonds in the bis[14]annulene topologies show a higher degree of bending based on molecular modeling calculations.

The energy of the charge-transfer optical band gap is further minimized in donor/acceptor-substituted DBAs **15**−**19**. Bathochromic shifts of ∼60 nm are observed for the longest wavelength absorptions of the planar annulenes over the nonplanar donor/acceptor-functionalized TPEBs with absorption cutoffs extending past 600 nm (Figure 7). The DBAs with linear-conjugated pathways all display two large, broad peaks, while the low-energy absorption of annulene **17**, lacking linear-conjugated pathways, is distinctly reduced. Little change in the wavelengths of the higher energy bands was noticed with

Scheme 7

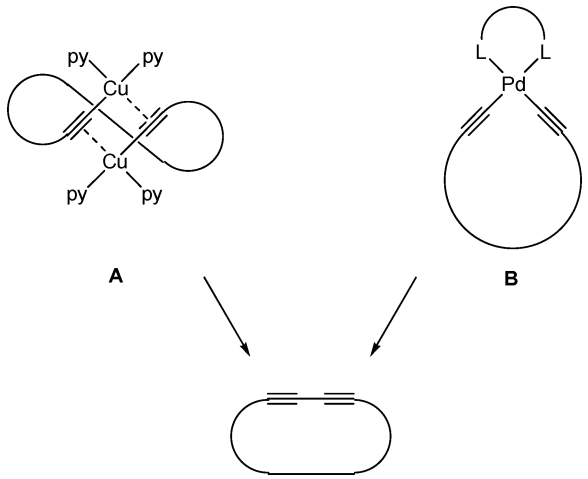

changes in donor/acceptor substitution or planarity. Similar to the TPEB series, meta fusion of donor and acceptor groups on the DBA's central phenyl ring (**17** and **19**) gave rise to the largest, most red-shifted charge-transfer band with a similar correlation in the calculated net dipole moments.

Protonation of the NBu_2 substituents by concentrated aqueous HCl showed a marked affect on the UV−vis spectra of the tetra-donor and donor/acceptor TPEBs and DBAs. Upon protonation,

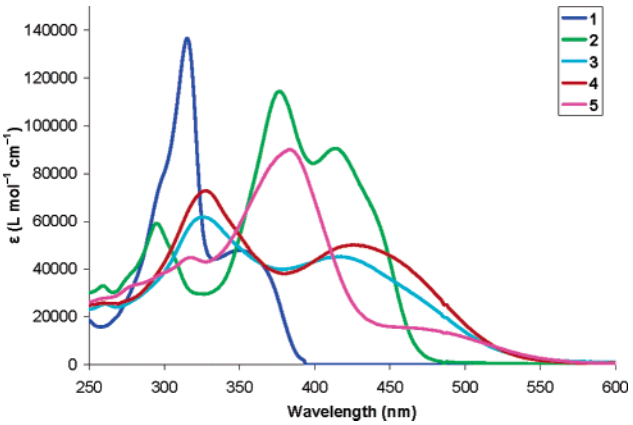

Figure 4. UV−vis spectra of TPEBs **1**−**5**.

Table 3. UV−Vis Data for TPEBs and DBAs

compound	peak 1 λ_{max} (nm) (ϵ [L mol^{-1} cm^{-1}])	peak 2 λ_{max} (nm) (ϵ [L mol^{-1} cm^{-1}])	cutoff (nm)	net dipole (D)[a]
1	316 (136 900)	350 (47 800)	395	0.00
2	377 (119 500)	414 (94 300)	481	0.00
2·HCl	318 (128 200)	349 (46 600)	395	*b*
3	326 (61 800)	417 (45 200)	565	18.51
4	328 (72 800)	426 (50 100)	565	13.24
4·HCl	316 (53 300)	346 (61 100)	426	*b*
5	317 (44 800)	383 (90 100)	567	0.00
11	307 (105 900)	417 (51 900)	438	0.00
12	343 (129 700)	419 (11 000)	434	0.00
13	330 (100 000)	472 (101 500)	507	0.00
13·HCl	307 (134 300)	422 (28 000)	447	*b*
14	323 (107 700)	463 (94 400)	499	0.00
15	319 (58 400)	456 (30 100)	600	15.06
16	318 (99 200)	491 (57 300)	600	18.34
16·HCl	308 (113 600)	430 (46 400)	470	*b*
17	330 (91 300)	473 (29 400)	620	0.00
18	326 (71 200)	453 (34 400)	600	15.26
19	325 (68 700)	466 (40 600)	600	18.33

[a] Calculated using the B3LYP/6-31G* basis set. [b] Not calculated.

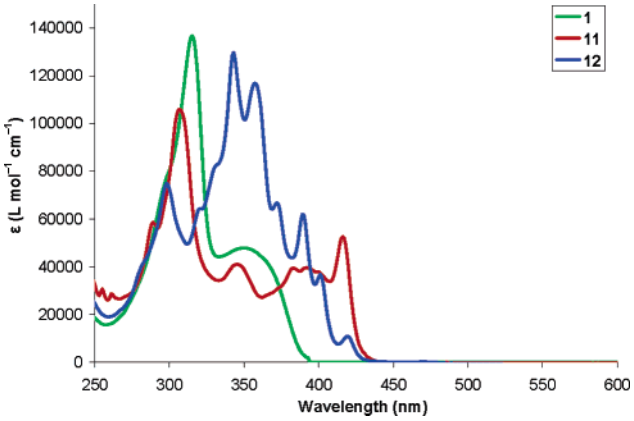

Figure 5. UV−vis spectra of neutral TPEB **1** and DBAs **11** and **12**.

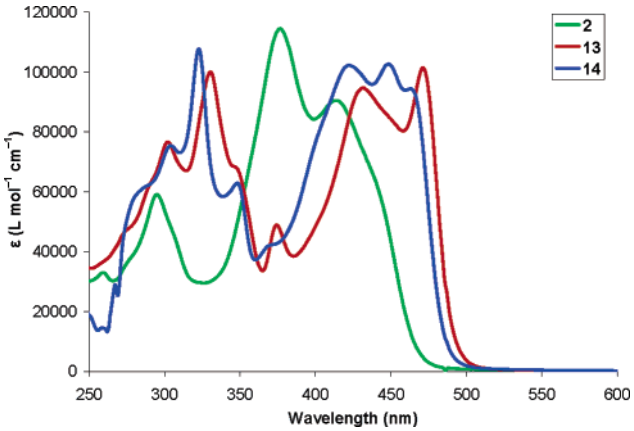

Figure 6. UV−vis spectra of tetra-donor TPEB **2** and DBAs **13** and **14**.

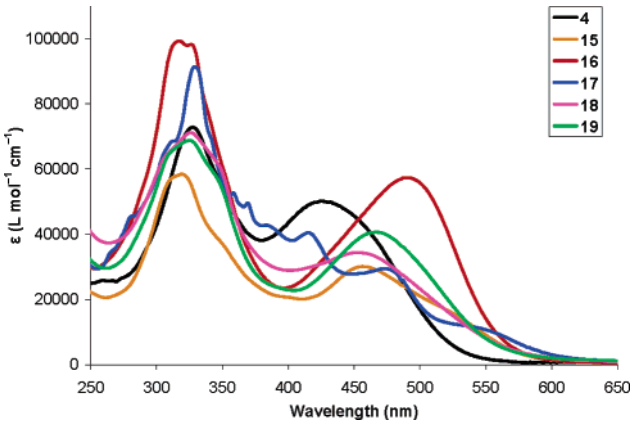

Figure 7. UV−vis spectra of donor/acceptor TPEB **4** and DBAs **15**−**19**.

the low-energy charge-transfer bands were effectively quenched. As can be seen in Figure 8, protonation completely disrupted any electron-donating capability of the donor groups. The absorption bands of the protonated form of TPEB **2** closely match that of the unsubstituted parent TPEB **1**, with hypsochromic shifts of the low-energy bands of more than 60 nm. Treatment of the protonated species of **2** with aqueous NaOH regenerated its neutral form, demonstrating the reversibility of the process.

Similar shifts due to protonation were also observed in the electronic absorption spectra of the DBA systems. Protonation of tetra-donor **13** eliminated the low-energy peaks and matched the spectrum of the neutral tetra-decyl DBA **11**. The disappearance of the charge-transfer bands of the donor/acceptor-functionalized DBAs by protonation was also readily observable. Although red-shifted by ∼15 nm, the absorption spectrum of **16** after acidic treatment closely resembled that of neutral **11**, suggesting that the influence of the nitro acceptor groups alone is minor.

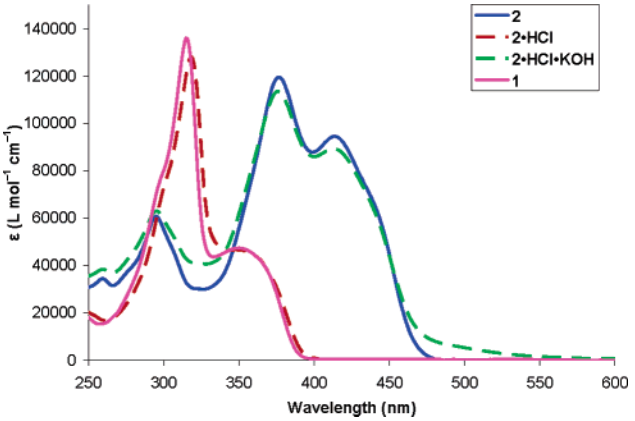

Figure 8. Protonation/deprotonation of TPEB **2**.

Table 4. Fluorescence Data for TPEBs and DBAs

compound	solvent	λ_{em} (nm)	Stokes shift (nm)	Φ_F[a]
1	CH_2Cl_2	505	154	0.02
	PhMe	506	157	0.02
2	CH_2Cl_2	512	98	0.71
	PhMe	507	98	0.22
2·HCl	CH_2Cl_2	562	213	0.09
	PhMe	508	164	0.01
3	PhMe	547	79	0.30
11	CH_2Cl_2	513	97	0.25
	PhMe	513	97	0.23
12	CH_2Cl_2	504	85	0.14
	PhMe	508	89	0.18
13	CH_2Cl_2	541	72	0.21
	PhMe	528	63	0.38
13·HCl	CH_2Cl_2	513	91	0.18
	PhMe	511	94	0.02
14	CH_2Cl_2	513	63	0.57
	PhMe	513	63	0.43
15	PhMe	565	113	0.11
16	PhMe	560	75	0.17
16·HCl	CH_2Cl_2	517	88	0.31
17	PhMe	580	109	0.06
18	PhMe	560	114	0.10
19	PhMe	560	97	0.09

[a] Measured with reference to fluorescein or 3-aminofluoranthene.

Fluorescence Spectroscopy of the TPEBs and DBAs. A strong fluorescence emission was observed for the majority of the TPEB and DBA systems. The degree of red-shift in their emission spectra closely matched the shift patterns observed in the electronic absorption spectra, with relatively large Stokes shifts and λ_{em} values ranging from 505 to 580 nm (Table 4). Discrete differences in emission energy and quantum efficiency based on the electronics and planarity of each system were observed. A dramatic solvent dependency was also observed, due to the highly polarized excited states. Through control of the structural elements of the molecules as well as the solvent systems used, a broad range of emissions across the visible spectrum was achieved (Figure 9). Indeed, a mixture of tetradecyl **11**, TPEB **3**, and DBA **17** in solution gave a bright "white" emission, demonstrating the ability to "tune" the systems for desired optical properties.

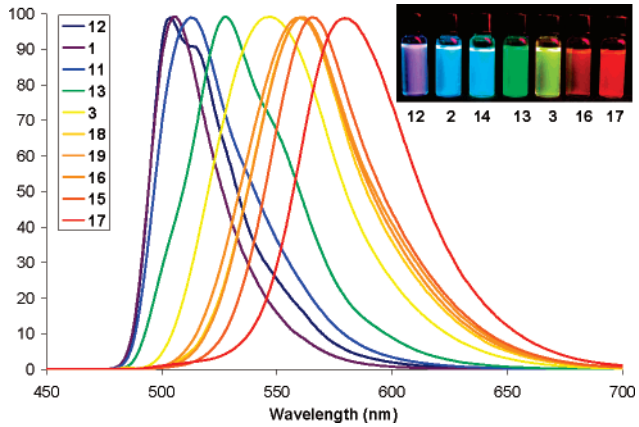

Figure 9. Fluorescence emission of selected TPEBs and DBAs.

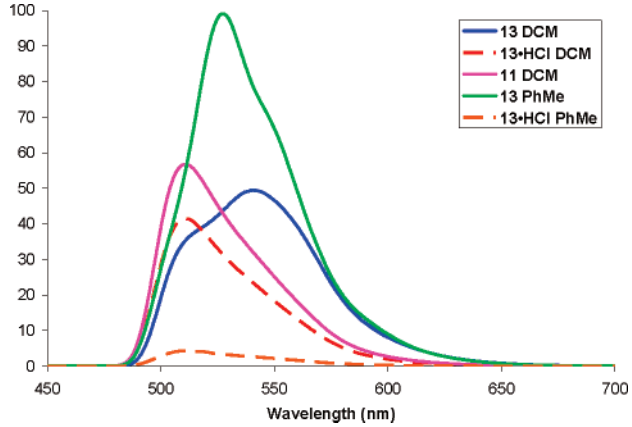

Figure 10. Emission consequences of protonation of DBA **13**.

The emission λ_{max} was very similar for the neutral systems **1**, **11**, and **12** in both CH_2Cl_2 and toluene, and little difference in quantum efficiency was noticed between solvents (Table 4). The increased conjugation and planarity of the annulene systems, on the other hand, allowed much higher quantum yields (Φ_F = 0.20−0.32) than the surprisingly low value for the nonplanar TPEB **1** ($\Phi_F \approx 0.02$) and was highest for the bis[15]annulene **11**. However, this trend was completely different for the tetra-donor-substituted species **2**, **13**, and **14**, which showed dramatic solvent and structural dependence. The highest quantum yield measured in this study belonged to TPEB **2** in CH_2Cl_2 (Φ_F = 0.71), while its efficiency was nearly 3.5 times lower in toluene. Interestingly, the tetra-donor bis[14]annulene **14** (Φ_F = 0.57, 0.43) demonstrated a much higher quantum efficiency than bis-[15]DBA **13** (Φ_F = 0.21, 0.38) with a reversal in solvent effect. For the donor/acceptor-substituted systems, solvent effects dictated the quantum efficiencies over structural differences. Very little fluorescence occurred for these systems in polar solvents because of stabilization of the charge-transfer excited state, which is minimized in more nonpolar solvents, allowing higher emission efficiencies through other pathways. Hence, very low quantum yields (<0.01) were observed for the donor/acceptor TPEBs apart from the ortho-substituted TPEB **3** in toluene (Φ_F = 0.30). Similarly, in CH_2Cl_2 low efficiencies (<0.01) for the donor/acceptor DBAs were measured, while in the less polar solvent toluene, an increase in the quantum yield to Φ_F = 0.06−0.17 was seen.

Protonation of the NBu_2 groups also resulted in distinct changes in the emission spectra of the molecules, although the effects were remarkably different for each system. Treatment of the tetra-donor TPEB **2** with concentrated aqueous HCl in both CH_2Cl_2 and toluene effectively diminished and red-shifted the emission (Table 4). However, more complex, solvent-dependent energy levels were present in the annulene systems. The emission peak of protonated tetra-donor DBA **13** in CH_2Cl_2 remained intense (Φ_F = 0.18) with a blue-shift to identically match the emission spectra of the neutral DBA **11**, while in toluene a larger quenching of the fluorescence emission was observed (Figure 10, Table 4). Donor/acceptor DBA **16** proved to be an interesting system for study. In its neutral form, a modest emission was observed in toluene (Φ_F = 0.17), while very little fluorescence occurred in CH_2Cl_2 (Φ_F > 0.01). Conversely, the protonated form of **16** gave an intense emission in CH_2Cl_2 (Φ_F = 0.31) with minute fluorescence in toluene (Φ_F > 0.01). These results demonstrate the importance of solvent parameters for fluorescence spectroscopy.

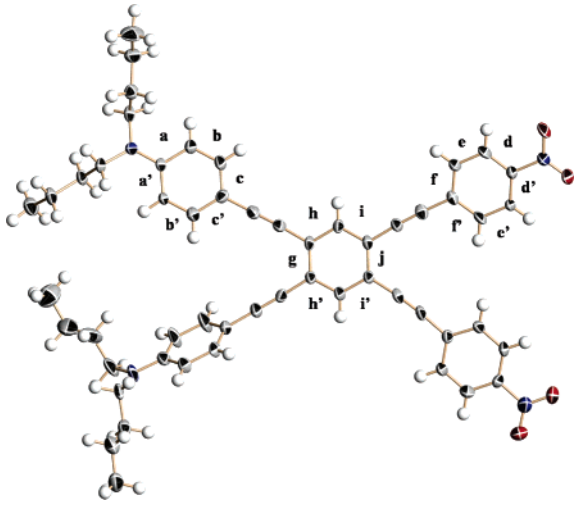

Figure 11. ORTEP representation of **3** at the 50% probability level.

Computational Studies. Further insight into the electronic nature of the TPEB and DBA systems can be attained through computational studies. Geometry optimization provided us with additional information regarding the conjugation effectiveness in order to better understand the differing charge-transfer pathways (Figure 1) and structural topologies present in each system. Examination of the molecular orbital diagrams provided further insight into the charge transfer and $\pi-\pi^*$ transitions and the relationship between the HOMO−LUMO gaps and the absorption energies present in the UV−vis spectra of each system.

Geometry Optimization. Geometry optimization calculations were performed with the B3LYP/6-31G* basis set.[22] All NBu_2 groups were replaced with NMe_2 groups, and all decyl groups were replaced with protons to reduce calculation time and should have little effect on overall electronics and geometry. Slightly shorter bond lengths, with good overall correlation, were seen between the calculated bond lengths of **2** and **3** and those experimentally obtained from their X-ray crystal structures (Figure 11), validating the accuracy of the calculations.[22]

The calculated bond lengths and their alternation can provide a great deal of information about the degree of charge transfer present between the donor and acceptor groups in the ground state. The bond length alternation can be expressed in terms of

the quinoid character (δr) of each aryl ring and is an indicator of the extent of charge transfer present along the conjugated backbones (eq 1; see Figure 11 for explanation of *a*, *b*, and *c*).[13,28] Fully aromatic with no quinoid character, the δr value of benzene is 0, while values of 0.08−0.10 are typical for fully quinoidal rings.

$$\delta r = \frac{((a + a')/2 - (b + b')/2) + ((c + c')/2 - (b + b')/2)}{2} \quad (1)$$

Interesting trends were observed for the δr values obtained from the calculated bond lengths of the TPEBs and DBAs (tabulated in Supporting Information). Values for the donor/acceptor-functionalized TPEB systems (**3** and **4**) displayed the highest quiniodal character ($\delta r = 0.028-0.029$ for the donor rings), followed by the bis[14]annulenes (**18**−**20**, $\delta r = 0.025-0.026$ for the donor rings), and finally the bis[15]annulenes (**15**−**17**, $\delta r = 0.024$ for the donor rings). While these numbers are comparable to δr values obtained for tetraethynylethylenes (TEEs) with NMe_2 donor groups containing similar pathways,[6] the trend for each series is in disagreement with the data obtained from UV−vis measurements and would indicate a reversal of the charge-transfer efficiency. This anomaly most likely arises from an oversimplification of the defined quinoid pathways existing in the DBA systems. Because of the large number of conjugated pathways other than donor to acceptor and the structural differences between each macrocycle, a competition arises for conjugation between the charge-transfer pathways and the fused 14- or 15-membered rings. Bond length distortion due to ring strain may also have an appreciable effect on bond length alternation. Nevertheless, good agreement between UV−vis data and quinoid values was observed between the neutral (**1**, **11**, and **12**), tetra-donor (**2**, **13**, and **14**), and donor/acceptor-substituted TPEBs and DBAs (**3**−**5** and **15**−**20**) with an increase in the δr value going from neutral to tetra-donor to donor/acceptor system. A correlation between the degree of red-shift from the electronic absorption spectra and the largest quinoid value for each series was also seen, with the meta-substituted isomers (**4**, **16**, and **19**) displaying the largest degree of charge transfer.

Crystals of **2** and **3** suitable for X-ray structure analysis were grown by slow diffusion of hexanes into CH_2Cl_2 solutions. Although bond lengths were slightly shorter overall, quinoid values of **2** and **3** measured from the X-ray crystal data matched those obtained from calculations quite well (Supporting Information). However, the average δr value for **3** was much smaller than calculated, because of the considerable out-of-plane twisting of one phenyl ring in the solid state (up to ca. 70°, Figure 11). This twisting greatly reduced the conjugation effectiveness and charge-transfer ability of the donor/acceptor conduit, resulting in a negative quinoid value ($\delta r = -0.0055$) for that pathway, while the planar pathway displayed a quinoid value close to that calculated in the gas-state assuming total planarity ($\delta r = 0.0234$). This indicated again the importance of planarity for effective charge transfer in these systems.

Also of interest was the crystal packing of **3**, which shows alternating slipped stacks with unidirectional alignment of the dipole in each layer.[22] The dipolar alignment in alternating layers is opposing, thus creating an overall centrosymmetric packing arrangement. The stacking distance between planes of 3.71 Å is similar to the distance observed for a slipped parallel arrangement of a benzene dimer.[29]

Molecular Orbital Plots. The molecular orbital plots displayed a marked difference between the electronic transitions of the neutral and tetra-donor systems versus the donor/acceptor-functionalized phenylacetylenes. Analysis of the calculated absorption maxima showed the first excited state for the TPEBs and DBAs to comprise mainly an electronic transition between the HOMO and the LUMO.

Strong delocalization was present in the HOMOs of both the neutral (**1**) and tetra-donor (**2**) TPEB systems (Figure 12). However, the LUMOs show more localization of the isosurfaces of the wave functions around the central benzene, with weaker delocalization moving outward toward the peripheral phenyl rings illustrating significant π*-antibonding character. In contrast to the neutral and tetra-donor species, the donor/acceptor TPEBs (**3**−**5**) exhibit strong charge-transfer transitions from the HOMO to the LUMO. The orbitals in the HOMOs reside wholly at the donor-substituted phenyls and weaken down the ethynyl bonds to the central benzene ring. In the LUMOs it is transferred to the opposing ends of the charge-transfer pathways and is localized at *p*-nitrophenyl acceptors. Interestingly, the para-substituted species **5**, lacking linear-conjugated pathways, shows the most complete localization of the isosurface between the donor and acceptor units of the molecule, which may explain the longer absorption cutoff in its UV−vis spectrum.

Characteristics similar to the TPEBs were observed for the HOMO and LUMO plots of the DBA systems (Figure 12). Tetra-decyl **11** showed complete delocalization of the orbitals around the macrocycle and phenyl rings in the HOMO, which becomes more localized to the π*-antibonding orbitals in the LUMO. Tetra-donor DBA **13** displayed slightly more localization on the central cruciform backbone in the HOMO and more localization on the outer diacetylene bridges of the LUMO. Analogous to the TPEB systems, the donor/acceptor DBAs (**15**−**17**) show strong charge transfer from the donor to the acceptor for the HOMO−LUMO transition. Relatively little isosurface is present on the diacetylene bridges in any of the orbital plots of the donor/acceptor DBAs, indicating that this linker has little contribution to conjugation and exists solely for planarization of the system. Molecular orbital plots of the analogous bis[14]-annulenes (not shown) displayed similar characteristics to the bis[15]annulenes, also highlighting the distinct differences between the $\pi-\pi$* transitions of the neutral and tetra-donor systems and the charge-transfer transitions of the donor/acceptor DBAs.

There existed some discrepancy between the HOMO−LUMO transitions from ab initio calculations and the experimentally obtained optical gaps acquired from UV−vis spectroscopy in CH_2Cl_2 that must be rationalized. The calculated absorption maxima for all neutral and tetra-donor systems showed a correlation of ±30 nm. The calculated wavelengths for the nonplanar species were longer than the experimental, while the DBA systems were shorter (Table 5). The higher energy of the calculated optical energy gap in the neutral and tetra-donor DBAs could suggest that the lowest energy transition may not

(28) Dehu, C.; Meyers, F.; Brédas, J. L. *J. Am. Chem. Soc.* **1993**, *115*, 6198−6206.

(29) Tsuzuki, S.; Honda, K.; Uchimaru, T.; Mikami, M.; Tanabe, K. *J. Am. Chem. Soc.* **2002**, *124*, 104−112.

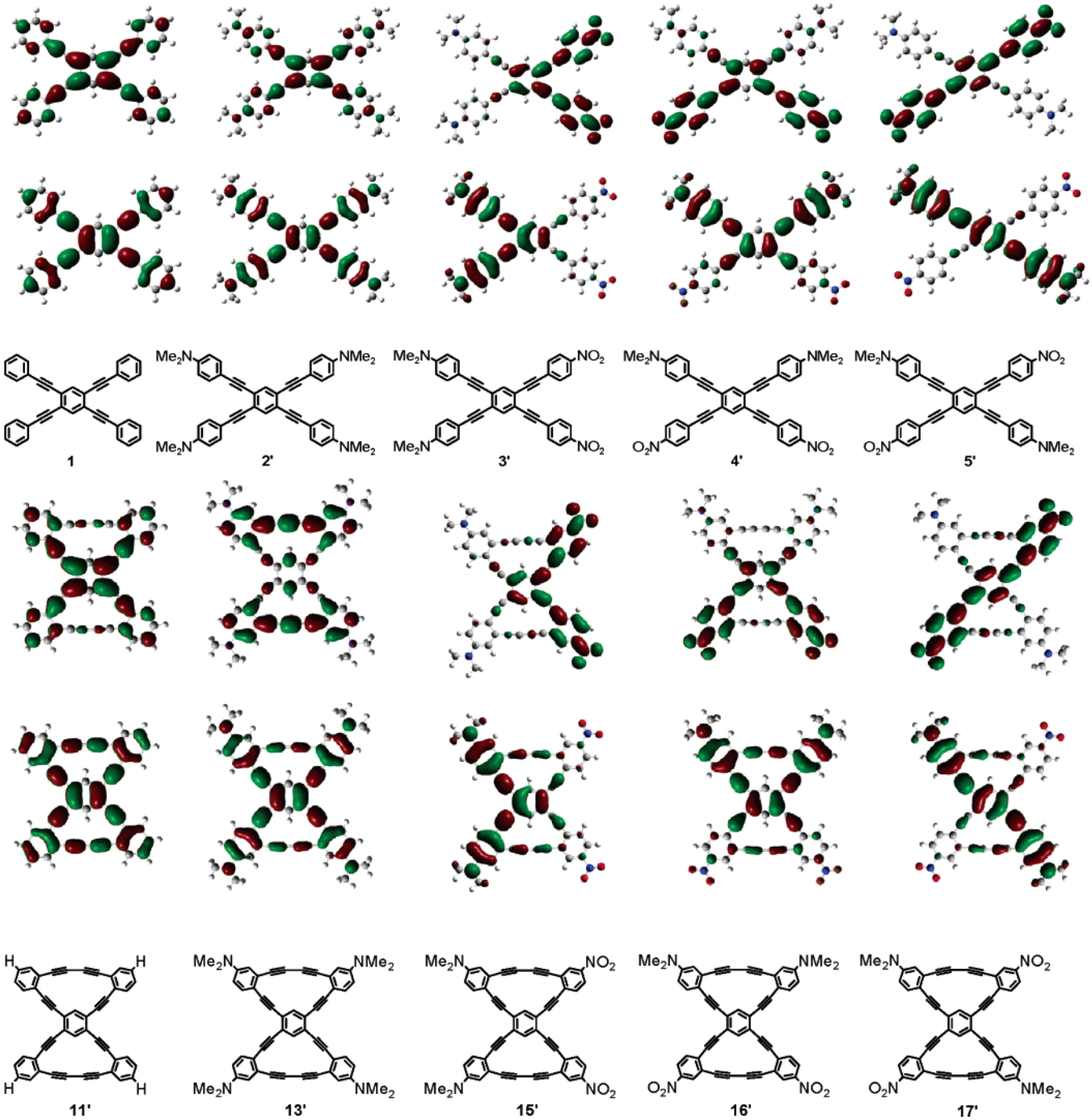

Figure 12. Molecular orbital plots of simplified structures of TPEBs **1**−**5**′ and DBAs **11**′, **13**′, and **15**′−**17**′. The upper plots represent the LUMOs, and the lower plots represent the HOMOs.

be due to a HOMO−LUMO transition. The larger amount of fine structure present in the UV−vis spectra of these annulenes suggests more complex energy transitions (Figures 5 and 6). The calculated energy levels of the HOMOs for the tetra-donor systems were ca. 1.0 eV higher than the neutral species. Also of interest were the lower energy HOMOs of the bis[14]-annulenes over the bis[15]annulenes (0.1−0.2 eV), suggesting that more strain or other energy may be present in the 15-membered rings and that the aromaticity of the 14-membered rings may also help stabilize the systems.

The calculated HOMO−LUMO gaps for the donor/acceptor-functionalized species were on average 100-nm longer than the experimentally obtained absorption maxima (Table 5). The lowest energy absorptions for these systems, however, appear very broad and do extend well beyond the calculated values (Figures 4 and 7). The trends between isomers for the calculated optical gaps are also dissimilar from the experimental data. Calculations show the highest energy transitions belonging to the meta isomers (**4**, **16**, and **19**), which demonstrate the lowest energy UV−vis absorptions. The lowest energy absorptions from calculations belong to the para isomers, which do possess red-shifted shoulders extending beyond the other isomers (Figure 7). Although the variance between calculated and experimental data was large in some cases, overall the B3LYP/6-31G*

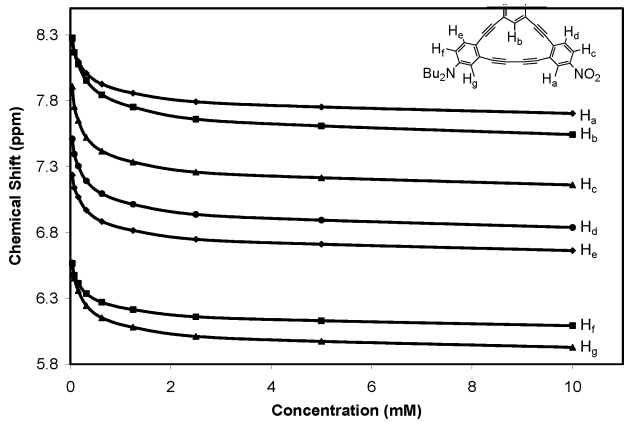

Figure 13. Concentration-dependent chemical shifts of the aromatic protons of DBA **15** in CD_2Cl_2 at 20 °C.

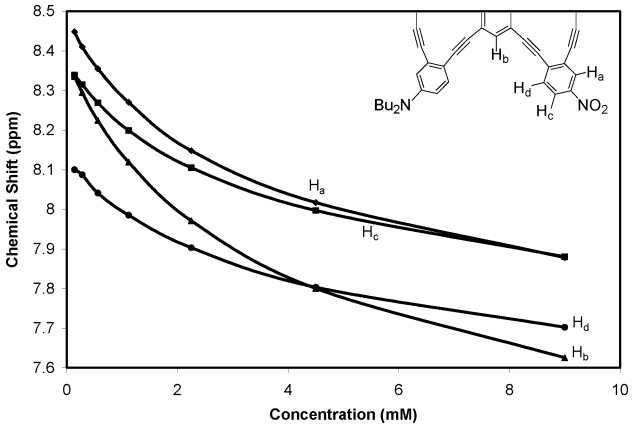

Figure 14. Differences in concentration-dependent chemical shifts of selected aromatic protons of DBA **18** in CD_2Cl_2 at 20 °C.

Table 5. Calculated (B3LYP/6-31G*) and Experimental HOMO−LUMO Band Gaps for TPEBs **1**−**5** and DBAs **11**−**20**

	calcd[a]				exptl
	E(HOMO)	*E*(LUMO)	Δ*E*(L–H)	λ (nm)	λ (nm)
1	0.00	+3.21	3.21	386	350
2	+1.03	+3.97	2.94	422	414
3	+0.30	+2.53	2.23	555	417
4	+0.19	+2.61	2.42	512	426
5	+0.32	+2.50	2.18	570	383[b]
11	+0.11	+3.13	3.02	411	417
12	-0.22	+3.02	3.24	383	419
13	+1.01	+3.78	2.78	447	472
14	+0.82	+3.78	2.97	418	463
15	+0.25	+2.45	2.20	563	456
16	+0.16	+2.53	2.37	524	491
17	+0.27	+2.40	2.12	584	473[c]
18	+0.11	+2.40	2.29	542	453
19	-0.03	+2.50	2.53	490	466
20	+0.14	+2.36	2.23	556	NA

[a] Values in electronvolts relative to **1**. [b] Shoulder at 480 nm. [c] Shoulder at 550 nm.

calculations provided insight into trends in the strength and type of transitions.

Self-Association of Donor/Acceptor Macrocycles in Solution. During routine examination and characterization of donor/acceptor-functionalized macrocycles **15**−**19** by ^{1}H NMR spectroscopy, very large concentration-dependent chemical shifts were observed for the aromatic protons (over ca. δ 1 ppm for the range of 0.1−10 mM). This observation suggested the occurrence of self-association in solution by π-stacking to form dimers or larger aggregates. Aggregation was also detectable in the UV−vis spectra of concentrated samples of donor/acceptor DBAs as a broadening and red-shift of the absorption bands.[22] This self-association phenomenon is well-known for functionalized, ethynyl-bridged metacyclophanes[30−35] and hexa(arylethynyl)benzene derivatives,[36] but has not been observed for dehydrobenzoannulene systems. Self-association such as described by weak noncovalent interactions including π-stacking and donor/acceptor interactions are an important aspect of supramolecular chemistry.[30−37] Therefore, we decided to further investigate the aggregation properties of the donor/acceptor DBAs to gain insight into their self-association characteristics and to identify trends in aggregation propensity, if any, for each unique isomer and ring topology.

The self-association properties of the DBAs and TPEBs were investigated quantitatively by analysis of the concentration-dependent ^{1}H NMR chemical shifts of the aromatic protons and further verified by vapor phase osmometry (VPO). ^{1}H NMR spectroscopy is the most widely used technique for analyzing aggregation behavior because of its ease of measurement, good precision, and for the secondary benefit of providing structural information pertaining to the aggregates.[38] The ^{1}H NMR method cannot, however, distinguish between dimer and higher aggregate formation, necessitating VPO measurements. Significant concentration-dependent chemical shifts were observed for each of the donor/acceptor-functionalized annulenes in a variety of solvents. For example, upfield shifts of the aromatic protons of more than δ 0.7 ppm were observed for DBA **15** in CD_2Cl_2 at 20 °C as the concentration was increased from 0.04 to 10 mM (Figure 13). The strong propensity for aggregation even at very low concentration can be seen, suggesting a large association constant. The upfield character of the protons and little chemical shift change at concentrations above ∼2.0 mM are indicative of this propensity, while below ∼2.0 mM concentration the chemical shifts move sharply downfield. No concentration-dependent chemical shifts were observed for the neutral or tetra-donor DBAs or the TPEBs with or without donor and acceptor groups. This difference indicates that both planarity and donor and acceptor substitution are necessary for aggregation in these materials.

To calculate the association constants (K_2), we assumed that the monomer−dimer equilibrium was the predominant process and verified this assumption by VPO, as will be described later. To determine K_2, the chemical shifts at various concentrations were curve-fitted to eq 2,[39] where δ is the chemical shift at substrate concentration C_t, and δ_m and δ_d are the chemical shifts

(30) Tobe, Y.; Utsumi, N.; Kawabata, K.; Nagano, A.; Adachi, K.; Araki, S.; Sonoda, M.; Hirose, K.; Naemura, K. *J. Am. Chem. Soc.* **2002**, *124*, 5350−5364.
(31) Nakamura, K.; Okuba, H.; Yamaguchi, M. *Org. Lett.* **2001**, *3*, 1097−1099.
(32) Höger, S.; Bonrad, K.; Mourran, A.; Beginn, U.; Möller, M. *J. Am. Chem. Soc.* **2001**, *123*, 5651−5659.
(33) Lahiri, S.; Thompson, J. L.; Moore, J. S. *J. Am. Chem. Soc.* **2000**, *122*, 11315−11319.
(34) Shetty, A. S.; Zhang, J.; Moore, J. S. *J. Am. Chem. Soc.* **1996**, *118*, 1019−1027.
(35) Zhang, J.; Moore, J. S. *J. Am. Chem. Soc.* **1992**, *114*, 9701−9702.
(36) Kobayashi, K.; Kobayashi, N. *J. Org. Chem.* **2004**, *69*, 2487−2497.
(37) (a) Roesky, H. W.; Andruh, M. *Coord. Chem. Rev.* **2003**, *236*, 91−119. (b) Claessens, C. G.; Stoddart, J. F. *J. Phys. Org. Chem.* **1997**, *10*, 254−272. (c) Philp, D.; Gramlich, V.; Seiler, P.; Diederich, F. *J. Chem. Soc., Perkin Trans. 2* **1995**, 875−886. (d) Hunter, C. A. *Chem. Soc. Rev.* **1994**, 101−109. (e) Desiraju, G. R. *Crystal Engineering: The Design of Organic Solids*; Elsevier: New York, 1989. (f) Foster, R. *Organic Charge-Transfer Complexes*; Academic Press: London, 1969.
(38) Martin, R. B. *Chem. Rev.* **1996**, *96*, 3043−3064.
(39) Horman, I.; Dreux, B. *Helv. Chim. Acta* **1984**, *67*, 754−764.

Table 6. Association Constants (K_2) and Solubilities of Donor/Acceptor-Functionalized DBAs at 20 °C

	CD_2Cl_2		THF-d_8		$CDCl_3$		PhMe-d_8	
	K_2 (M^{-1})	solubility	K_2 (M^{-1})	solubility	K_2 (M^{-1})	solubility	K_2 (M^{-1})	solubility
15	3020 ± 360	10 mM	1090 ± 310	3 mM	1540 ± 660	12 mM	605 ± 240	2 mM
16	1940 ± 290	20 mM	294 ± 53	6 mM	5000 ± 3000	1.5 mM	*b*	>0.1 mM
17[a]	*b*	0.8 mM	*b*	1.2 mM	2600 ± 860	10 mM	748 ± 348	20 mM
18	129 ± 10	25 mM	29.3 ± 8.4	15 mM	121 ± 6	15 mM	186 ± 66	5 mM
19	326 ± 51	25 mM	52.0 ± 7.8	15 mM	172 ± 35	15 mM	300 ± 48	10 mM

[a] Calculated using the infinite association model (see below). [b] Solubility too low for calculation of K_2.

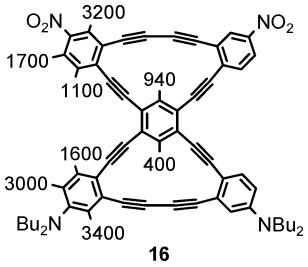

16

Figure 15. Associations constants (K_2) of aromatic protons of DBA **16** in $CDCl_3$ at 20 °C.

of the monomer and dimer, respectively.

$$\delta = \delta_m + (\delta_d - \delta_m)\left(1 + \frac{1 - \sqrt{8K_2C_t + 1}}{4K_2C_t}\right) \qquad (2)$$

The association constants were calculated for each of the aromatic protons present in DBAs **15**−**19** in $CDCl_3$, CD_2Cl_2, THF-d_8, and PhMe-d_8. A large variance of the concentration-dependent chemical shift was seen for several DBAs depending on the local environment of each proton as can be seen in the dilution curve of DBA **18** (Figure 14). Typically exo-annular protons exhibited the largest association constants, while intraannular protons, or protons residing in the "pocket" between rings showed a much smaller K_2, as illustrated for DBA **16** (Figure 15). The association constants of all aromatic protons were averaged for each annulene, giving values summarized in Table 6 along with the solubility data for each system. In general, the bis[15]annulenes (**15**−**17**) showed an association constant about 1 order of magnitude larger than that of the bis-[14]annulenes (**18** and **19**) and were also much more soluble in the solvents used for the measurements. Solubility had a significant effect on the K_2 values and the error associated with the data because of the smaller range of solute concentrations achievable for measurement (Table 6). Solvent polarities have previously been observed to have a crucial effect on self-association.[30,32,33] Not surprisingly, the DBAs with larger net dipoles were generally much more soluble in polar solvents. For example, macrocyle **16** with the largest calculated dipole of 18.34 D demonstrated increasing solubility as solvent polarity increased, while DBA **17** with no net dipole had much better solubility in less polar solvents. We also found that more polar solvents, in general, saw enhancement of K_2. Interestingly, association constants were also generally higher in halogenated solvents ($CDCl_3$ and CD_2Cl_2) than nonhalogenated (THF-d_8 and PhMe-d_8). The bis[14]annulenes **18** and **19**, moreover, saw an increase of K_2 in PhMe-d_8. Similar observations have also been made for *m*-phenyleneethynylene macrocycles in aromatic solvents.[30,31,33]

To verify the usage of the dimer model for self-association, average aggregate size was determined by VPO. Osmotic

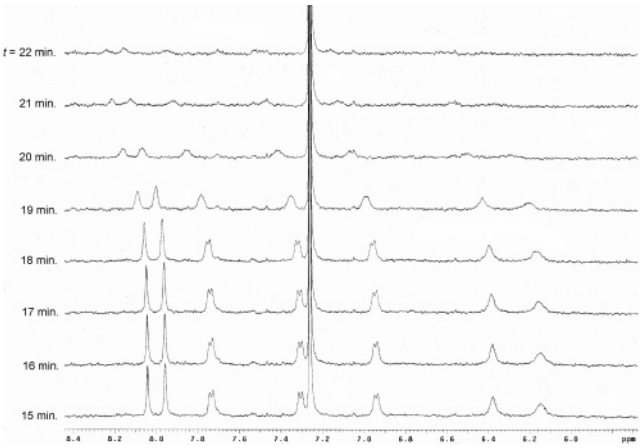

Figure 16. Polymerization of DBA **17** in $CDCl_3$ observed by ^1H NMR.

measurements were performed in $CHCl_3$ at 40 °C using benzil and TPEB **2** as standards. The stoichiometric molal concentrations were calculated from the solute weights, and the colligative molal concentrations were obtained by comparing their VPO readings against those of benzil and TPEB **2**.[34,40] The colligative molal concentrations of **15**, **16**, **18**, and **19** with solute concentrations between 1.0 and 5.0 mM were consistent with aggregate sizes of dimers, while DBA **17** strongly indicated aggregates much larger than dimer. Thus, the association constants for **17** were calculated using the infinite association model assuming $K_2 = K_3 = K_4 = ... = K_n$.[30,38]

During the investigations into the self-association properties of the donor/acceptor-functionalized macrocycles, an interesting phenomenon was observed for the para-substituted DBA **17**. Although stable in the solid state, in $CDCl_3$ or $CHCl_3$ solutions greater than ~1.0 mM at room temperature a facile polymerization occurred that could be monitored by ^1H NMR (Figure 16). The aromatic chemical shifts progressed downfield with time, indicating a decrease in concentration until after about 20 min, no annulene was left in solution, and an insoluble red-brown polymer precipitated out. We were unable to find an organic solvent in which the resulting precipitate was soluble, making analysis difficult. SIMS-TOF mass spectrometry of the material showed broad repeating humps, indicating polymeric material. Powder X-ray diffraction of this polymer suggested an ordered polymerization, showing very sharp peaks with the largest representing a repeat distance of ~21.5 Å, roughly the distance across the macrocycle. Therefore, what is most likely occurring is a topochemical 1,3-diacteylene polymerization[26,41]

(40) Schrier, E. E. *J. Chem. Educ.* **1968**, *45*, 176−180.
(41) (a) Shirakawa, H.; Masuda, T.; Takeda, K. In *The Chemistry of the Triple-Bonded Functional Groups*; Patai, S., Rappoport, Z., Eds.; Wiley: New York, 1994; pp 704−728. (b) Enkelmann, V. *Adv. Polym. Sci.* **1984**, *63*, 91−136. (c) Wegner, G. *Pure Appl. Chem.* **1977**, *49*, 443−454. (d) Wegner, G. *Z. Naturforsch* **1969**, *24b*, 824−832.

driven by preorganization from the self-association. This is a well-known phenomenon involving cyclic and other 1,3-diacetylenes, although it is typically observed in the solid state. Strangely, this polymerization occurs only with the para isomer (**17**) and, of the solvents tested, only in $CDCl_3$ or $CHCl_3$. Acid-catalyzed polymerization was ruled out because no difference was observed between $CHCl_3$ pretreated with K_2CO_3 and untreated $CHCl_3$ containing trace amounts of acid. Although we have not been able to explain the selectivity for DBA **17**, polymerization may explain the difficulties associated with synthesis of the elusive DBA **20** containing the same para substitution of donor and acceptor groups. Because of the added strain energy on the diacetylenes of the bis[14]annulenes, polymerization of **20** may be even more facile than **17** and occur before isolation of the DBA is possible.

Conclusions

We have synthesized a series of tetrakis(phenylethynyl)-benzenes, bis(dehydrobenzo[14]annuleno)benzenes, and bis-(dehydrobenzo[15]annuleno)benzenes functionalized with all neutral, all donor, or mixed donor/acceptor groups to compare the electronic and optical properties between each species to develop a structure−function relationship. During this synthesis, an interesting selectivity between ring sizes was found based on reagents used in the cyclization. We noticed an enhancement of the optical activity transitioning from neutral to tetra-donor to donor/acceptor systems as seen by large bathochromic shifts of the UV−vis λ_{max} and the development of strong charge-transfer bands. Further enhancement was achieved by locking the nonplanar TPEBs into planarity as DBAs, thereby increasing overall conjugation. As observed for previous donor/acceptor systems, we found that larger net dipoles and linear-conjugated pathways provided the largest bathochromic shifts. We were able to tune the optical fluorescence emission of the series over a broad range of the visible spectra, and we established that the tetra-donor compounds provided the best efficiency for fluorescence. In both absorbance and emission, protonation of the donor groups quenched or altered the optical enhancements.

Through computational studies, further insight into the electronic transitions was gained. A distinct difference was found between the $\pi-\pi^*$ transitions of the neutral and tetra-donor systems and the charge-transfer transitions of the donor/acceptor compounds as seen by the molecular orbital plots. The degree of quinoid character of the system was calculated and observed to correlate well with experimental measurements of charge-transfer effectiveness.

Self-association properties for the donor/acceptor DBAs to form dimers based on face-to-face $\pi-\pi$ stacking in solution were also observed, and the association constants were measured. Both donor and acceptor substitution as well as planarity were necessary for self-association. The geometry of the ring was found to be a large factor in aggregation propensity, as the 15-membered rings showed around 1 order of magnitude larger association constants. An interesting ordered polymerization triggered by self-association was observed for only one isomer (**17**) in only $CDCl_3$, suggesting that the reaction is very sensitive to geometrical and solvent effects. We are continuing our studies on donor/acceptor pathways through experiments involving macrocycles of different sizes and saturations and degree of donor and acceptor substitution, and we will report these results in due course.

Acknowledgment. This work was supported by the National Science Foundation (CHE-0414175). J.A.M. and L.D.S. acknowledge the NSF for IGERT fellowships. We thank Elliott Hinds for help acquiring some characterization data and Dr. Grant Palmer for preliminary synthetic studies. We thank Drs. Fusen Han and Elizabeth Rather for the X-ray crystallography of **2** and **3**.

Supporting Information Available: Experimental section. Detailed experimental procedures and spectral data for all new compounds and their intermediates, computational details, quinoid calculations, and self-association ^1H NMR and UV−vis data (CIF, PDF). This material is available free of charge via the Internet at http://pubs.acs.org.

JA044175A